Geochemical Perspectives Letters

A global imbalance in potassium and barium river export: the result of biological uptake?

Q. Charbonnier, J. Bouchez, J. Gaillardet, E. Gayer, S. Porder

Supplementary Information

The Supplementary Information includes:

- 1. Sample Set and Sampling Methodology
- 2. Analytical Methods
- 3. Global Input of Barium to the Ocean
- 4. Derivation of Catchment-Scale Mass and Isotope Budget Equations
- 5. Testing for a "Poorly Gauged Flux" as an Explanation of the Observed Imbalance in Rock-Derived Nutrients in River Exports
- 6. Testing for a "Growing Organic Pool" as an Explanation of the Observed Imbalance in Rock-Derived Nutrients in River Exports
- Tables S-1 to S-3
- Figures S-1 to S-7
- Supplementary Information References

1. Sample Set and Sampling Methodology

The sampling locations of the rivers analysed in this study are presented in Figure S-1. Most river samples come from the sample repository of Institut de Physique du Globe de Paris, and were collected over the 1990–2000 decades during various sampling campaigns (Gaillardet *et al.*, 1999a, 1999b; Lemarchand *et al.*, 2000; Tipper *et al.*, 2006, 2010). Time series from Arctic rivers and from the Congo Basin were collected by other research groups (Holmes *et al.*, 2012; Spencer *et al.*, 2012). Altogether, this dataset includes the Congo and Niger rivers in Africa, the Brahmaputra, Ganges, Hong He, Irrawaddy, Mekong, Narmada, Salween, and Tapti rivers in southeast Asia; the Changjiang, Huang He, and Xijiang rivers in China, the Amazon, Madeira, Solimões, Negro, and Orinoco rivers in South America; the Fraser, Kolyma, Lena, Mackenzie, Nass, Ob, St-Lawrence, Stikine, Yenisey, and Yukon rivers in the Arctic region; and the Seine in Europe. The cumulative water discharge represented by this

data set (letting aside the Solimões, Madeira, and Negro which are tributaries of the Amazon, already featured in the sample set) is around 36 % of the global water discharge to the ocean, and their cumulative surface represents 37 % of the continental surface draining to the oceans (Milliman and Farnsworth, 2011).

Classically, river water is filtered immediately after collection through 0.2-µm porosity cellulose acetate or poly-ether sulfone filters, using Teflon-coated, under-pressure filtration units. Filtered river water represents the dissolved load, while suspended sediments are retrieved from the filter, but note that in the present study as in many others, colloidal matter (that is, solids in suspension but with size <0.2 µm) is operationally considered to be part of the dissolved load. Because of their low hydrolysis constant, the four soluble elements considered here (Na, Li, K, Ba) are not likely to be strongly complexed to organic colloids nor present in significant amount in colloidal-sized clay particles. However, a significant fraction of the insoluble element loads used for normalization in the mass budget equations (section S-4) such as Th, can be present in this colloidal fraction, which can generate some bias for rivers rich in colloids, as discussed below.

Importantly for the topic addressed in the present study, because with the adopted sampling scheme in most large river studies, with a typical volume of a river water sample is in the range 0.5 to ~10 L, large organic debris (macrophytes, trunks) cannot be sampled, and their contribution to the river POC export is missed by this sampling scheme. However, fine organic material, being associated to minerals or transported as small organic debris, can be retrieved on filters (Galy *et al.*, 2008).

2. Analytical Methods

Both the elemental and isotope data for river dissolved and solid loads are reported in Table S-1.

2.1 Major and Trace Element Determinations

Major and trace element concentrations of river sediments were measured by ICP-AES and ICP-MS, respectively, at the SARM (Service d'Analyse des Roches et des Minéraux, INSU facility, Vandoeuvre-les-Nancy, France; analytical details available at http://helium.crpg.cnrs-nancy.fr/SARM). Major cation and anions of the dissolved load were

measured using ionic chromatography, while dissolved silica has been measured using UV-Vis spectrophotometry. Trace elements in the dissolved load were measured using ICP-MS, all at the High-Resolution Analytical Platform (PARI) of IPGP. Except for Ba abundance, all major element concentration data are from Lemarchand *et al.* (2000).

2.2 Isotope Measurements

For the present study, only barium (Ba) stable isotope ratios were analysed, as all other isotope measurements (lithium: Li) were already reported in previous studies (Dellinger *et al.*, 2014, 2015a, 2015b, 2017; Wang *et al.*, 2015; Henchiri *et al.*, 2016). The protocols for Ba separation and isotope measurements are described in Charbonnier *et al.* (2020). Briefly, a minimum of 200 ng Ba for each sample was separated from the sample matrix by ion chromatography (AG50W-X8 resin) using 2.5 N HCl to elute the matrix and 6 N HCl to elute Ba. For each sample, the separation procedure was performed two times to ensure a complete purification. The isotopic ratios were measured by MC-ICP-MS (Thermo Fisher Scientific, Neptune) at the PARI analytical platform of IPGP. Mass instrumental fractionation was corrected for using sample-standard bracketing. The interference of Xe on mass 134 was corrected for by on-peak zeroes. Barium isotopic ratios in the samples and standards were measured as:

$$\delta^{x}\mathrm{Ba} = \left(\frac{\left(\frac{^{x}\mathrm{Ba}}{^{134}\mathrm{Ba}}\right)_{\mathrm{sample}}}{\left(\frac{^{x}\mathrm{Ba}}{^{134}\mathrm{Ba}}\right)_{\mathrm{standard}}} \right) \times 1000 \qquad \text{Eq. S-1}$$

with x = 137 or 138. The standard used in this study was the NIST SRM 3104a. For the sake of consistency, data were converted to $\delta^{138/134}$Ba assuming that $\delta^{138/134}\mathrm{Ba} \approx 1.33 \times \delta^{137/134}\mathrm{Ba}$. Uncertainties on δ^{138}Ba are reported as 95 % confidence interval following a Student distribution, and are typically between 0.04 and 0.20 ‰. The long-term accuracy of the data was checked using the JB-2 (0.04 ± 0.16, 2 s.d., n = 7), Babe27 (−0.80 ± 0.15, 2 s.d., n = 7), BHVO-2 (−0.01 ± 0.15, 2 s.d., n = 8) and AGV-2 (0.05 ± 0.15, 2 s.d., n = 16) reference materials (Miyazaki *et al.*, 2014; van Zuilen *et al.*, 2016; Charbonnier *et al.*, 2018; Gou *et al.*, 2020).

3. Global Input of Barium to the Ocean

The isotope cycle of Ba has recently gained momentum due to its potential for reconstructing the strength of the ocean biological pump through geological timescales (Horner *et al.*, 2015; Bridgestock *et al.*, 2018, 2019), but the use of this proxy requires constraining the riverine input of Ba to the ocean. Below, because of the novelty of these Ba isotope data, we provide an analysis of the dissolved and solid riverine fluxes of Ba from the world largest rivers.

3.1 Abundance and Isotope Signature of Ba in the Global Solid Riverine Export

The Ba abundance in river suspended sediments shows significant variation from 138 mg/kg (Narmada) to 948 mg/kg (Stikine). The Ba/Th ratio of river sediment which, unlike Ba concentration, is not affected by dilution by Ba free-phases such as quartz, ranges from 15 to 263, and thus for some rivers differs significantly from the upper continental crust (UCC) value (Ba/Th ≈ 50; Taylor and McLennan, 1995; Rudnick and Gao, 2014). The δ^{138}Ba values of river suspended sediments (denoted $\delta^{138}Ba_{spm}$ in the following, 'spm' standing for "suspended particulate matter") vary between −0.14 and +0.34 ‰, whereas that of riverbed sediments (called $\delta^{138}Ba_{rbs}$ hereafter) range from −0.25 to +0.36 ‰ (Table S-1, Fig. S-2). River material $\delta^{138}Ba_{spm}$ values are thus significantly different from the Ba isotope composition the UCC (0.00 ± 0.04 ‰; Nan *et al.*, 2018). For any given river, $\delta^{138}Ba_{spm}$ and $\delta^{138}Ba_{rbs}$ are close to one another, suggesting a relative invariance of sediment Ba isotope composition despite grain size variations (Bouchez *et al.*, 2011), in contrast with results for other isotope systems (Dellinger *et al.*, 2014; Garçon *et al.*, 2014) but in agreement with observations made for Ba from river depth profiles in the Amazon Basin (Charbonnier *et al.*, 2020). Nonetheless, the wide δ^{138}Ba range of the solid load is quite surprising regarding the relative homogeneity of δ^{138}Ba in the rock forming the UCC and the weathering product of other large rivers (Nan *et al.*, 2018; Charbonnier *et al.*, 2020; Gou *et al.*, 2020).

3.2 Abundance and Isotope Signature of Ba in the Global Dissolved Riverine Export

The Ba abundance in the dissolved load varies from 0.05 µmol/L (Yenisey) to 0.76 µmol/L (HuangHe) and an average of 0.21 µmol/L (Table S-1), similar to the world average of 0.17 µmol/L estimated by Gaillardet *et al.* (2014).

However, Ba abundance in the dissolved load is likely influenced by water dilution. A way to cancel out this dilution effect is to normalise the Ba concentration to that a conservative element, here sodium (Na*), where "*" refers to the Cl-based correction from sea salt and halite inputs (Gaillardet *et al.*, 1997). Across our dataset, Ba/Na^* ratios also vary widely from 0.0001 (Irrawaddy) to 0.022 (Rio Negro).

The fraction of total Ba river transport that occurs as dissolved species can be calculated as follows:

$$w^X = \frac{[X]_{\text{diss}}}{[X]_{\text{diss}} + [X]_{\text{spm}} \times [\text{spm}]} \quad \text{Eq. S-2}$$

with $[X]_{\text{diss}}$ the dissolved concentration of X (*e.g.*, in µg/L), $[X]_{\text{spm}}$ the concentration of X in the river sediment (*e.g.*, in mg/kg) and [spm] the concentration of suspended sediment in the river (in g/L). In this study we use the long-term (typically multi-decadal) estimates of [spm] provided by (Milliman and Farnsworth, 2011).

The dissolved phase represents on average 20 % of total river Ba (*i.e.* $w^{Ba} \approx 0.2$; Fig. S-3, Table S-2). However, the global range of variation of w^{Ba} is very large: for some rivers, mainly those characterised by low erosion rates such as the Congo Basin, almost all Ba is transported in the dissolved load ($w^{Ba} \approx 0.86$), whereas in highly erosive contexts such as in the Huang He Basin, river Ba is entirely transported as solids ($w^{Ba} \approx 0.01$). The $\delta^{138}Ba$ values of the dissolved load of large rivers ($\delta^{138}Ba_{diss}$) range from −0.02 to +0.80 ‰ (Table S-1, Fig. S-2), on average significantly higher than that of the UCC (0.00 ± 0.04 ‰; Nan *et al.*, 2018). This first-order observation suggests that at the continental scale, the Ba dissolved flux to the ocean is influenced by processes such as secondary phase formation or biological uptake; by the release from rock types unaccounted for in estimates of the UCC composition; or by a combination thereof.

3.3 The Isotope Composition of the Global Ba Flux to the Ocean

According to the global Ba fluxes reported by Gaillardet *et al.* (2014) and Viers *et al.* (2009), our river sample set represents 44 % (340×10^3 t yr^{-1} of 860×10^3 t yr^{-1}) and 30 % (2387×10^3 t yr^{-1} of 7835×10^3 t yr^{-1}) of the river Ba

dissolved and solid fluxes to the ocean, respectively. These numbers indicate that our dataset is representative of the global riverine export of Ba.

Our estimates for the Ba isotope composition of the global dissolved Ba flux ($\delta^{138}Ba_{diss,global}$) and solid Ba flux ($\delta^{138}Ba_{spm,global}$) are 0.24 ± 0.02 ‰ and 0.07 ± 0.03 ‰, respectively. Note that these isotope signatures are representative of the global Ba river fluxes before they enter estuaries, and thus can be affected afterward by estuarine processes (Bridgestock *et al.*, 2021).

The $\delta^{138}Ba_{diss,global}$ calculated from our study is slightly higher than the previously reported figure (0.16 ‰; Cao *et al.*, 2020). The reason for the higher $\delta^{138}Ba_{diss,global}$ found here stems from the presence of rivers having higher $\delta^{138}Ba_{diss}$ in our dataset such as the Mackenzie, Congo and other Arctic rivers. Nonetheless, for those rivers where the comparison can be made, we note that our values are similar to those of Cao *et al.* (2020).

4. Derivation of Catchment-Scale Mass and Isotope Budget Equations

In the present study, we establish catchment-scale mass budgets for the two non-nutrient elements lithium (Li) and sodium (Na), for the major nutrient potassium (K) (Chaudhuri *et al.*, 2007) and for a nutrient-like trace element: barium (Ba) (Bullen and Chadwick, 2016; Charbonnier *et al.*, 2020).

The fate of a chemical element after its release by rock dissolution can be investigated using so-called "catchment-scale" or "river mass" budgets (Gaillardet *et al.*, 1995; Stallard, 1995). In this approach, we test whether for an element X the sum of the river fluxes of dissolved material derived from chemical weathering (F^X_{diss}) and of sediment derived from physical erosion (F^X_{sed}) reflects the input of rock material to the Earth surface (F^X_{rock}):

$$F^X_{rock} = F^X_{diss} + F^X_{sed} \qquad \text{Eq. S-3}$$

If Equation S-3 is valid for an element X, the catchment-scale mass budget of this element can be qualified as "balanced". Conversely, a mismatch between the two sides of Equation S-3 indicates either (1) a poor estimate of F^X_{rock}, (2) that the river export fluxes F^X_{diss} and F^X_{sed} have not been properly measured, or (3) that rivers do not

currently export the exact amount of X supplied to the Earth surface (in other words, that the catchment is currently accumulating or losing X), or any combination thereof. In terms of absolute fluxes, the term F^X_{rock} of Equation S-3 is usually estimated from the sum of F^X_{diss} and F^X_{sed}, which can be difficult to obtain except in relatively rare occasions where suitable river gauging protocols are in place. To circumvent this issue, we introduce soluble-to-insoluble element ratios. Noting first that for an insoluble element Y, $w^Y \approx 0$:

$$F^Y_{\text{rock}} = F^Y_{\text{sed}} \qquad \text{Eq. S-4}$$

Dividing Equation S-3 by Equation S-4, and recognizing that the flux ratio $\frac{F^X_i}{F^Y_i}$ is equal to the elemental abundance ratio $\left(\frac{X}{Y}\right)_i$:

$$\left(\frac{X}{Y}\right)_{\text{rock}} = \frac{F^X_{\text{diss}} + F^X_{\text{sed}}}{F^Y_{\text{sed}}} = \frac{F^X_{\text{sed}}}{F^Y_{\text{sed}}} + \frac{F^X_{\text{diss}}}{F^Y_{\text{sed}}} = \left(\frac{X}{Y}\right)_{\text{sed}} + \frac{F^X_{\text{diss}}}{F^Y_{\text{sed}}} \qquad \text{Eq. S-5}$$

The right-hand side of Equation S-5 still features flux terms that are difficult to measure directly. We divide each side of Equation S-5 by $\left(\frac{X}{Y}\right)_{\text{rock}}$ and use Equation S-4:

$$1 = \frac{(X/Y)_{\text{sed}}}{(X/Y)_{\text{rock}}} + \left(\frac{F^X_{\text{diss}}}{F^Y_{\text{sed}}}\right) / \left(\frac{F^X_{\text{rock}}}{F^Y_{\text{rock}}}\right) = \frac{\left(\frac{X}{Y}\right)_{\text{sed}}}{\left(\frac{X}{Y}\right)_{\text{rock}}} + \frac{F^X_{\text{diss}}}{F^X_{\text{rock}}} = (1 + \tau_x) + w^X \qquad \text{Eq. S-6}$$

where $1 + \tau_x$ is the ratio between $(X/Y)_{\text{sed}}$ and $(X/Y)_{\text{rock}}$, and represents the relative depletion of X in river sediment with respect to the source rock (using for notation purposes the definition of the so-called "mass transfer coefficient" τ_x classically used in weathering studies at the soil scale; *e.g.*, Brimhall *et al.*, 1991). The

$1+\tau_x$ term also corresponds to the inverse of the α-depletion factor of soluble elements ($\alpha^X = \frac{(X/Y)_{\text{rock}}}{(X/Y)_{\text{sed}}}$) in river sediments defined by Gaillardet *et al.* (1999a). The ratio $\frac{F^X_{\text{diss}}}{F^X_{\text{rock}}}$ represents the relative transport of X as a dissolved species, that is equal to w^X defined in Equation S-2.

By definition, Equation S-6 is valid when the riverine export balances the amount of material supplied to the critical zone through rock degradation. If not, the imbalance is quantified as follows:

$$f^X_{\text{imbalance}} = 1 - (1+\tau_x) - w^X = -\tau_x - w^X \qquad \text{Eq. S-7}$$

If $f^X_{\text{imbalance}} > 0$, X is "less exported" by rivers than predicted by rock degradation. Conversely, if $f^X_{\text{imbalance}} < 0$, X is "more exported" by rivers than predicted.

In the present study we apply this approach to the nutrient(-like) elements K and Ba. In principle this can also be done for the other major cations Ca and Mg. Nevertheless, the significant contribution of carbonate to F^X_{rock} as well as F^X_{diss}, and to a lesser extent F^X_{sed}, makes it difficult to constrain their catchment-scale mass budgets. All results of Equation S-6 are reported in Figure 2 as a cross-plot of $(1+\tau_X)$ *vs.* w^X.

Although the introduction of element ratios in lieu of flux ratios in Equation S-3 mitigates the issues associated with the estimation of absolute fluxes, considerable uncertainty might stem from the fact that different rock types have different $(X/Y)_{\text{rock}}$ ratios. The first reason why $(X/Y)_{\text{rock}}$ ratios might differ between rock types is the differences in magmatic compatibility, which translates into variability in $(X/Y)_{\text{rock}}$ ratios between different types of crystalline rocks. In that respect, for a given soluble element X the best choice for the insoluble element Y is an element with a magmatic compatibility similar to that of X. In this study, following the approach of Gaillardet *et al.* (1999a) we use the Ba/Th, K/Th, Li/Al, and Na/Sm ratios.

The second reason why $(X/Y)_{\text{rock}}$ might differ between rock types is the depletion of meta-sedimentary rocks in soluble elements X compared to their crystalline protoliths, due to the fact that such rocks have already undergone loss of soluble elements during previous weathering episodes (Gaillardet *et al.*, 1999a). However, we first

note that the Ba/Th ratio of igneous rocks and shales are relatively similar. Only andesites, which are significantly present in the Solimões, Stikine and Nass basins, show a much higher Ba/Th ratio (Charbonnier *et al.*, 2020). In this case, we compute the $(Ba/Th)_{rock}$ ratio as a mixture between andesites and shales rocks using the relative rock contribution estimated by Dellinger *et al.* (2017). Potassium shows a relatively limited range of variation (from 28,000 to 33,083 mg/kg; Taylor and McLennan, 1995; Rudnick and Gao, 2014) between igneous rocks and shales. Therefore, we assume a single $(K/Th)_{rock}$ value of 2,500 for all rock types. The variability in Na abundance between meta-sedimentary and crystalline rocks is the highest (Taylor and McLennan, 1995; Rudnick and Gao, 2014), due to the high solubility of Na during weathering and the absence of reverse weathering reactions in the ocean involving Na. When possible, we use independent constraints on the bedrock undergoing weathering for the Amazon and its tributaries, the Congo, the Changjiang, the Mackenzie, and the Ganges-Brahmaputra systems from Dellinger *et al.* (2017). For rivers for which we do not have the required data, we assumed that the river bed sediment chemistry is representative of that of bedrock, as coarse sediment are thought to best represent the products of erosion of the rock undergoing degradation, but with no measurable effect of chemical weathering (Potter, 1978; Dellinger *et al.*, 2014).

The comparison between the catchment-scale mass budgets of elements of importance for plant nutrition with those of elements with no physiological role is a test for the influence of biological cycling on global river solute export. Previous studies have already suggested that at the global scale the river mass budgets of Li is balanced (Dellinger *et al.*, 2015a, 2017). However, we re-visit these results in the scope of detecting any pattern specific to the rock-derived nutrients K and Ba. Below, we provide a comparison of river mass budget results of K, Na, and Li as a function of Ba.

The two bio-utilised elements Ba and K show negative imbalance (the difference between what is supplied to the critical zone by rock degradation and the riverine export; see Eqs. S-6 and S-7) for most of the studied rivers (Fig. S-4a), the cause for which is discussed in the main text. Here, we point out the interesting feature that Ba and K riverine imbalance show a positive relationship, suggesting a common mechanism for their missing components (see main text), whereas no correlation emerges between the imbalance of Ba and Na (Fig. S-4b). The Li imbalance is hardly resolvable given the uncertainties, suggesting a balanced mass budget (Fig. S-4c). We note that for a few rivers, a positive imbalance is observed: there, the export of rock-derived nutrients outpaces

their supply to the Earth surface by the rock degradation. This is the case for the St. Lawrence River, where relatively recent ice cap retreat might result in an imbalance in the dissolved and solid riverine export (Gaillardet *et al.*, 1999a). In tropical rivers showing this type of positive imbalance, such as the Congo and Negro rivers, the presence of organic colloids enhanced the transport as a dissolved species of insoluble elements such as Th, thus compromising the use of Equation S-6 (Charbonnier *et al.*, 2020). In cold Arctic rivers such as the Fraser and the Mackenzie, source rocks may contain unaccounted-for rock sources of Ba—thought to be linked to the presence of black shale rocks in the catchment—that contribute to the riverine export (Guay and Falkner, 1998; Charbonnier *et al.*, 2022).

The same type of mass balance can be performed using isotope ratios (see Bouchez *et al.*, 2013). In such approach, the flux-weighted sum of the solid and dissolved isotope compositions should in principle be equal to the isotope composition of the rock undergoing weathering:

$$\delta^{X}_{\mathrm{rock}} = w^{X} \times \delta^{X}_{\mathrm{diss}} + (1 - w^{X}) \times \delta^{X}_{\mathrm{sed}} \qquad \text{Eq. S-8}$$

with $\delta^{X}_{\mathrm{rock}}$, $\delta^{X}_{\mathrm{diss}}$, and $\delta^{X}_{\mathrm{sed}}$ the isotope composition of element *X* in the rock undergoing weathering, the river dissolved load, and the river solid load, respectively. As for elemental mass balance, any difference between the value of $\delta^{X}_{\mathrm{rock}}$ calculated from river loads (right-hand side of Eq. S-8) and that estimated for bedrock from independent constraints (left-hand side of Eq. S-8) suggests that a fractionated reservoir of *X* is not exported by river, or at least not sampled properly in the river export.

Here, this calculation is performed for Ba and Li based on our own Ba data and Li data from Dellinger *et al.*, (2014, 2015b, 2017) and Wang *et al.* (2015) (see Table S-2). We took the estimation of the continental crust of Ba from Nan *et al.* (2018) for $\delta^{\mathrm{Ba}}{}_{\mathrm{rock}}$ since there is, on average, no significant variation between different rock types. $\delta^{\mathrm{Li}}{}_{\mathrm{rock}}$ are taken from (Dellinger *et al.*, 2017), as the isotope composition of bedrock Li can vary widely between catchments, due to the difference in Li isotope composition between igneous and sedimentary silicate rocks (Dellinger *et al.*, 2015a). Results are reported in Table S-2 and discussed in the main text.

5. Testing for a "Poorly Gauged Flux" as an Explanation of the Observed Imbalance in Rock-Derived Nutrients in River Exports

Here we test the hypothesis that part of the observed rock-derived nutrients imbalance is due to a "poorly gauged flux", as river export of coarse vegetation debris, in particular during high-flow events, is likely to be missed by classically-used sampling schemes of large rivers (see section S-1 above) (Abbe and Montgomery, 2003; Heartsill Scalley *et al.*, 2012; Wohl *et al.*, 2012; Uhlig *et al.*, 2017). To that effect, we first quantify the flux of river particulate organic carbon required to account for the observed riverine K imbalance (F^{C}_{miss}) following Charbonnier *et al.* (2020):

$$F^{C}_{miss} = \frac{F^{K}_{miss}}{(K/C)_{bio}} \quad \text{Eq. S-9}$$

with $(K/C)_{bio}$ the K/C ratio of the biological component exported by rivers (data from Charbonnier *et al.*, 2020); F^{C}_{miss} the required missing carbon flux, and F^{K}_{miss} the estimated missing potassium flux calculated as follows:

$$F^{K}_{miss} = D \times [K]_{rock} \times f^{K}_{imbalance} \quad \text{Eq. S-10}$$

with D the denudation rate D is the sum of the chemical weathering and physical erosion rates, typically estimated at the catchment-scale using either the river fluxes of weathering-derived solutes and sediments; or using the concentration of the cosmogenic nuclide beryllium-10 in river sands. Here it is used as a proxy for the rate at which rock is delivered to the Critical Zone at the catchment scale.

In Fig S-5, we compare the inferred carbon missing flux from Equation S-9 with independent constraints on particulate carbon riverine export (Galy *et al.*, 2015). This comparison is made using the relationships between POC export and the denudation rate D as (1) estimated from our own data on rock-derived nutrient (Eq. S-9) and (2) reported by Galy *et al.* (2015) from actual measurements of POC export. The relationship estimated from our data is two orders of magnitude higher than the observed relationship (Fig. S-5). This difference is likely too large to be realistic, suggesting that a poorly gauged POC flux alone is not responsible for the observed imbalance in rock-

derived nutrients catchment-scale mass budget.

Alternatively, tree logging by human activity could be responsible for such a poorly gauged flux. Nonetheless, river catchments characterised by the strongest negative imbalance in the river mass budgets rock-derived nutrients (Orinoco, Niger, Ganges-Brahmaputra) do not correspond to regions where deforestation is the most intense (Canada, Northern, Russia, Amazon plains and Congo Basin; Curtis *et al.*, 2018). Second, using the Global Forest Change map (Hansen *et al.*, 2013; https://glad.earthengine.app/view/global-forest-change), we quantified the relative forest lost from 2000 to 2020 for five basins: Amazon, Congo, Orinoco, Fraser, and Mackenzie. These basins feature different degrees of deforestation as well as different degrees of K depletion in rivers. The comparison between these two parameters does not show any meaningful relationship (see Fig. S-6). This first-order examination suggests that logging cannot account for the deleted K component of large river rivers.

A Limited Role of Anthropogenic Inputs to the K Riverine Budget

Regarding the potential role of fertiliser on the global K riverine budget, we first note that most of rivers show a depletion in K export, whereas any additional, non-accounted for source (such as fertiliser or atmospheric inputs) should lead to an excess of K in rivers. In addition, following the approach of Li *et al.* (2022), we compare the average NO_3/Na* and NO_3/K ratios for our rivers of 0.45 and 0.89, respectively, which are much lower than the anthropogenic signatures of fertilisers at NO_3/Na = 7 and NO_3/K = 4 (Chetelat *et al.*, 2008). In fact, across our dataset only the Changjiang shows a relatively high NO_3/K ratio of around 3. Of course, these elemental ratios only disclose the contribution of K-fertiliser to the dissolved load. However, given the high solubility of K-fertiliser (Mikkelsen, 2007), the latter should have a minor influence on the K river solid flux, that represents the main path of K riverine export. For these reasons, we assume that fertiliser should play a minor role in the K mass budget of large rivers.

6. Testing for a "Growing Organic Pool" as an Explanation of the Observed Imbalance in Rock-Derived Nutrients in River Exports

In this study, we explore the possibility that biological uptake is responsible for the observed widespread imbalance

in the riverine export of nutrient-like elements. One possible explanation might lie in short-term variability in the biota size at the catchment scale, which leads to net nutrient uptake or release. In particular, changes in the magnitude of the land carbon sink over the last decades (Pan *et al.*, 2011) might lead to imbalance in catchment-scale rock-derived nutrient export. As a test of this hypothesis, below we provide a derivation for quantifying the amount of the rock-derived nutrient that is taken up for a given increase in the size of the continental biota (in terms of total biomass), relative to the supply of this nutrient by rock degradation. We define the rate of increase of the size of the biota as:

$$r = \frac{d(M_{\mathrm{bio}})}{dt} \qquad \text{Eq. S-11}$$

where M_{bio} is the mass of the biota reservoir within a given large river catchment. Such an increase of the biota size is accompanied by an incremental flux of uptake of the nutrient X:

$$U^X = r \times [X]_{\mathrm{bio}} \qquad \text{Eq. S-12}$$

with $[\mathrm{X}]_{\mathrm{bio}}$ the concentration of X in the biota.

Then, normalizing U^X by the amount of X supplied by rock degradation yields the uptake of the nutrient X by the biota relative to the supply of X provided by rock degradation, a ratio hereafter called β:

$$\beta = \frac{r \times [X]_{\mathrm{bio}}}{D \times [X]_{\mathrm{rock}}} = \frac{F^X_{\mathrm{bio}}}{F^X_{\mathrm{rock}}} \qquad \text{Eq. S-13}$$

The β value is basically an estimate of the catchment-scale imbalance of X (as defined in Eq. S-7 above) that should be observed if the biomass in the catchment were increasing at a rate r, given a catchment-scale denudation D. Thus, calculated values for a given r can then be compared to observed estimates of X imbalance to assess the plausibility of the "growing organic pool" scenario. We calculate β for an incremental increase in the biota size of 0.1 and 0.2 % as estimated recently for the average yearly land C sink on the continents (Friedlingstein *et al.*, 2020), for a range of D of 10–500 t/km^2/yr as observed in most large river catchments (Milliman and Farnsworth, 2011; Wittmann *et al.*,

2020) for a range of elements (Al, B, Ba, Ca, Cu, Fe, Mg, Mn, Mo, Ni, P, K, Rb, Na, Sr, Zn) with different abundances in plants, ranging from essential nutrients to non-nutrient elements (Table S-3). We calculate $[K]_{bio}$ values using (a) a compilation for the chemical composition of plant parts from Charbonnier *et al.* (2020) and (b) a compilation for the chemical composition of leaves made in the frame of the present study. We plot the β value for K in Fig. S-7 as the latter is a major rock-derived nutrient for which we observed a riverine imbalance (Fig. 2). The order-of-magnitude difference between the two panels of Fig. S-7 is driven by the difference in the value of $[K]_{bio}$ used, showing how this calculation is sensitive to this poorly constrained parameter.

With this simple model, explaining the observed range K riverine imbalance (Fig. S-7) requires that $[K]_{bio}$ is higher than that proposed by Charbonnier *et al.* (2020). This is plausible as the compilation of Charbonnier *et al.* (2020) might be biased by an important number data entries of trunk samples, being characterised by lower concentrations of rock-derived nutrients compared to other plant tissues such as foliage. Conversely, the β value of K calculated with the foliage compilation should lead to an overestimation of the $[K]_{bio}$, thereby providing a "maximum" estimate. Therefore, although this calculation is subject to large uncertainties, it provides 1) a range of minimum and maximum uptake of K as a function of estimates for catchment-scale biomass growth denudation and 2) a first estimate for β values (as $[X]_{bio}$ remains hard to constrain) on major and trace elements at the Earth surface (see Tables S-3). This analysis shows that, except for elements such as Al or Na, biological cycling could in principle affects most of the elements and their isotope signatures exported by rivers. However, this requires a long-term growing organic pool to influence riverine export, of a magnitude that seems unlikely at the global scale (see main text).

Supplementary Tables

Table S-1 Elemental and isotope data on large rivers.

Table S-2 Results of the river mass budget calculations (Supplementary Information section 4).

Table S-3 Compilation of abundance of rock-derived nutrients in plants used to test for the "growing organic pool " scenario (Supplementary Information section 6).

Tables S-1 to S-3 are available for download (Excel) from the online version of the article at https://doi.org/10.7185/geochemlet.2214.

Supplementary Figures

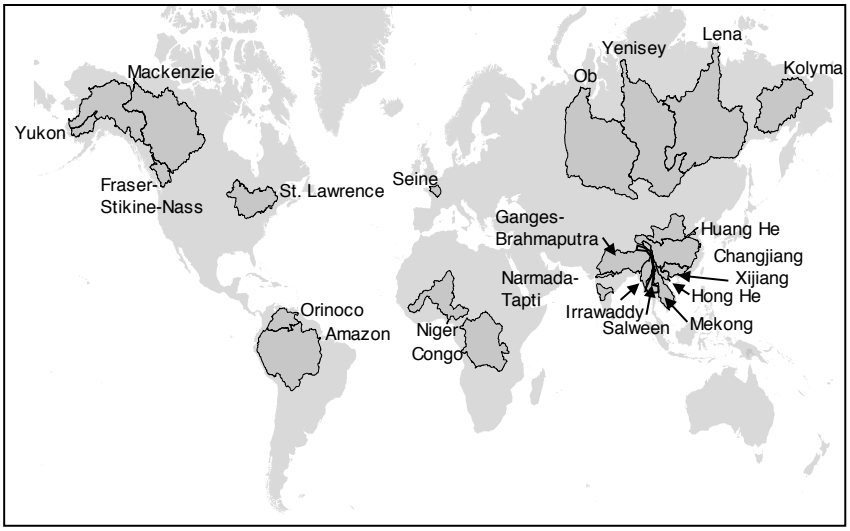

Figure S-1 World map showing the sample locations and river basins.

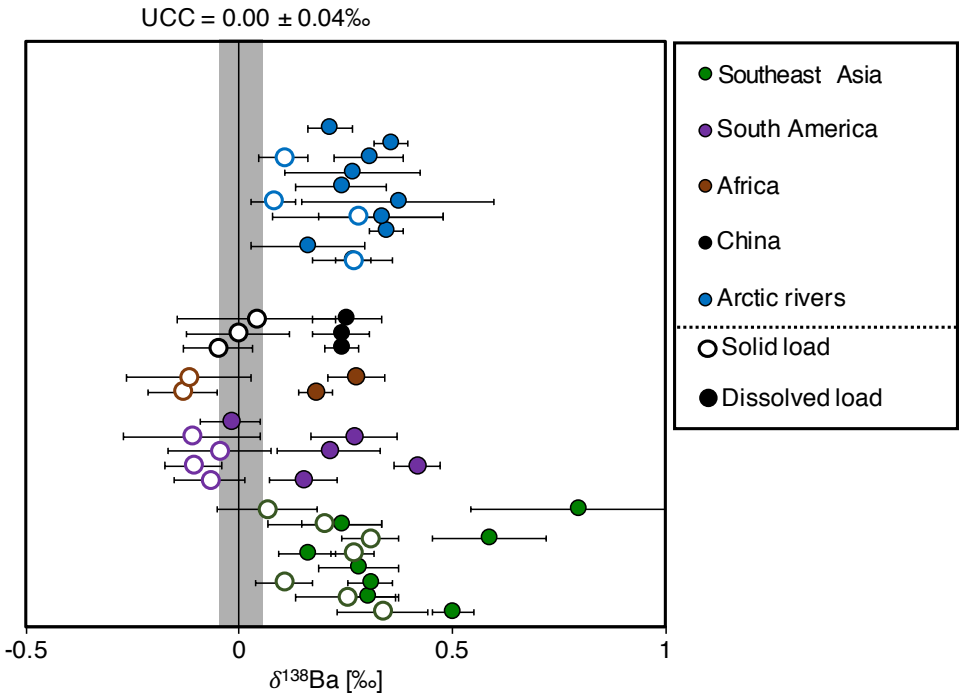

Figure S-2 Ba isotope composition of the dissolved and solid loads of the world's largest rivers. The value of the Upper Continental Crust (UCC), taken as the composition of the source rock, is derived from Nan *et al.* (2018).

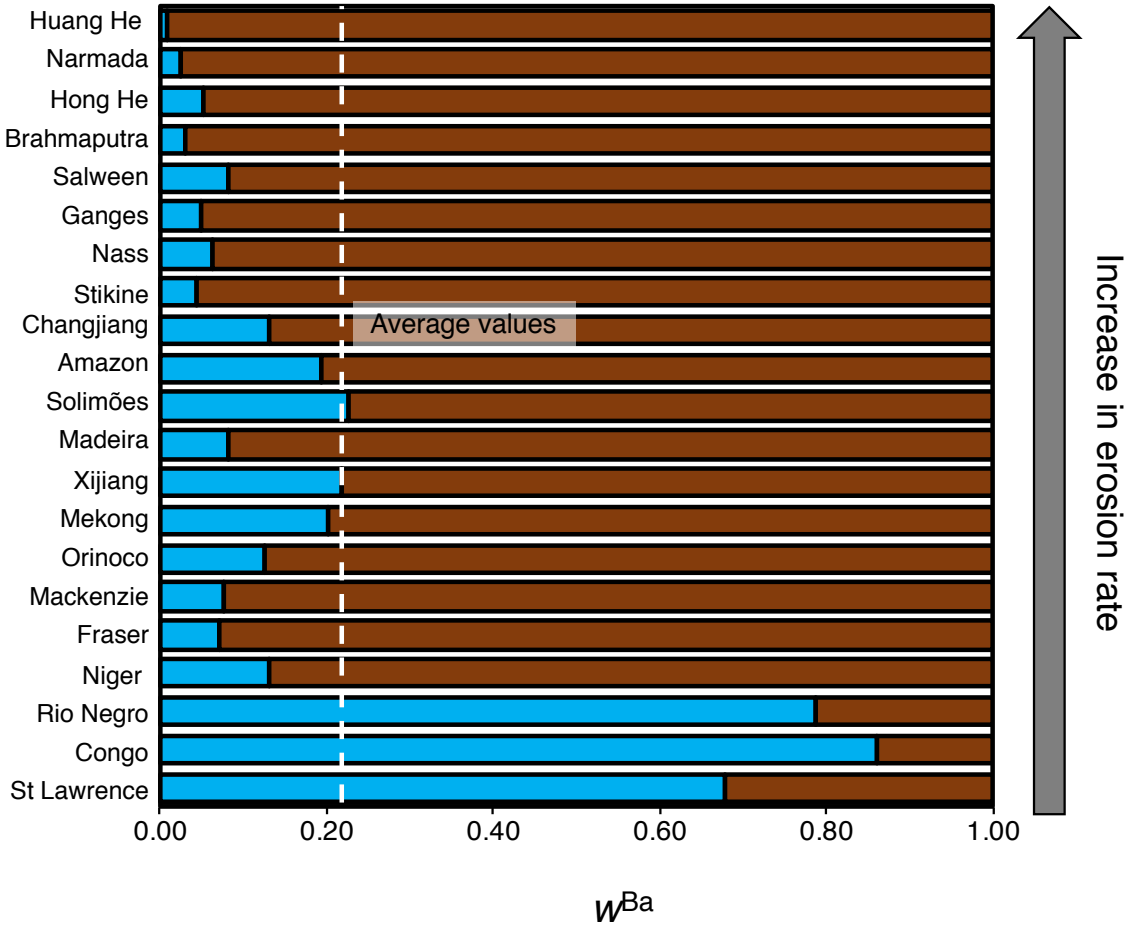

Figure S-3 Partitioning of Ba (w^{Ba}) between the river dissolved (blue) and the solid loads (brown) across the world largest rivers.

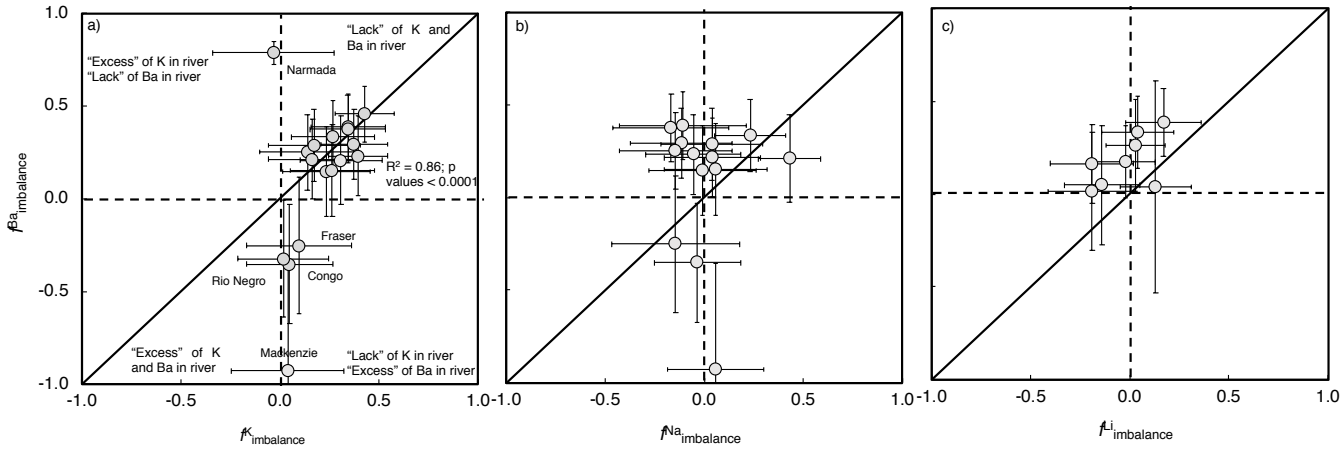

Figure S-4 Comparison of the Ba imbalance with **(a)** K imbalance, **(b)** Na imbalance, and **(c)** Li imbalance in their river mass budgets, as calculated using Equation S-7.

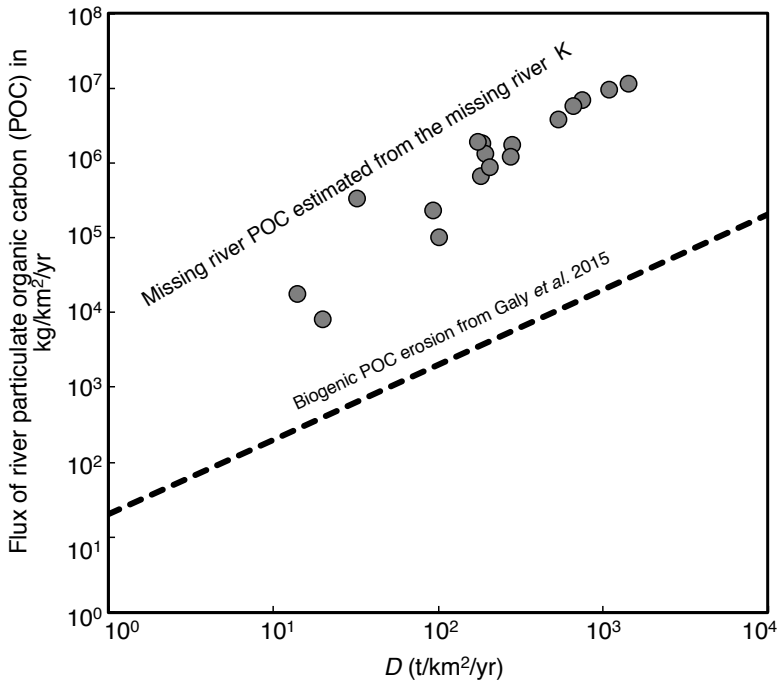

Figure S-5 Comparison of the relationship between denudation rate (D) and river particulate organic carbon (POC) flux estimated by Galy *et al.* (2015) from actual measurements of POC (black stippled line), and the same relationship calculated from catchment-scale mass budgets of rock-derived nutrients (Eq. S-9) shown as data points.

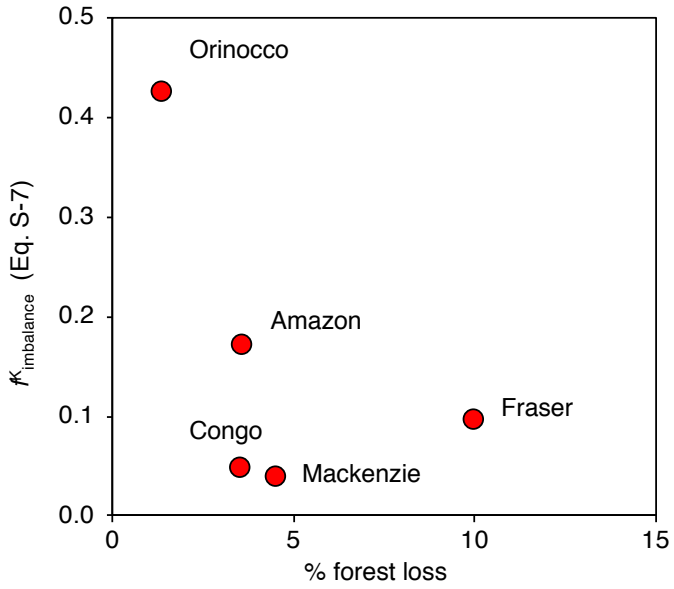

Figure S-6 Comparison between the relative K imbalance (quantified using Eq. S-7) and the relative forest loss during the last twenty years (2000–2020) using the Global Forest Change map (Hansen *et al.*, 2013; see Section 5).

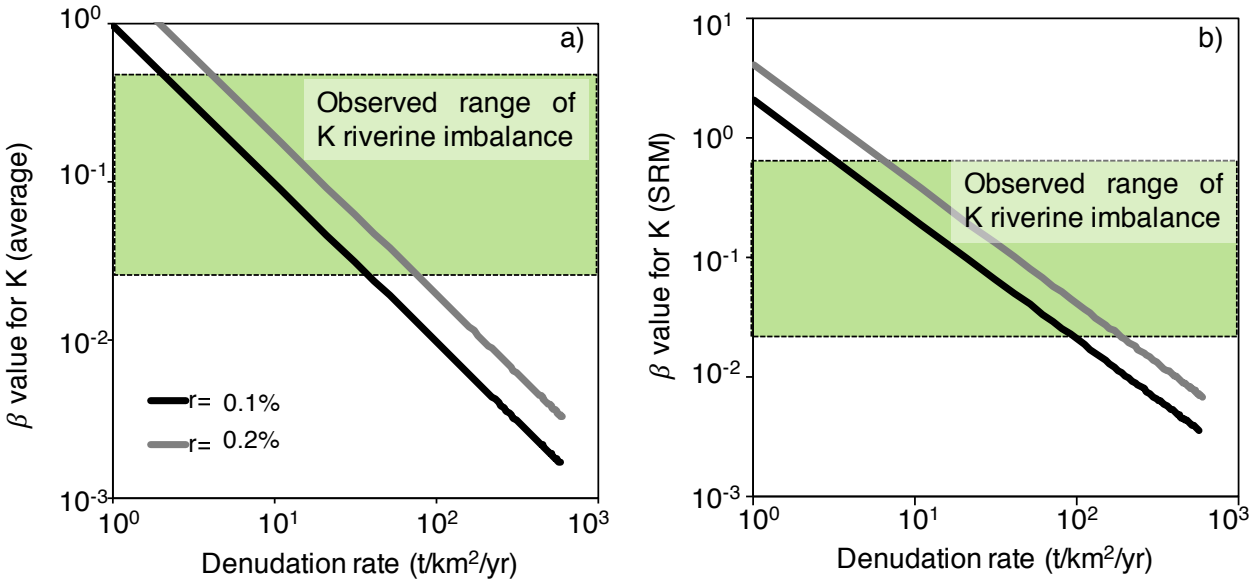

Figure S-7 β value (expected catchment-scale imbalance of a rock-derived nutrient in the case of biomass growth; Eq. S-13) of K for a denudation ranging from 10 to 500 t/km^2/yr. The green band indicates the range of K imbalance in the catchment-scale mass budgets of large rivers, as computed from Equation S-7. In the legend, r corresponds to the yearly relative rate of biomass growth. Results presented in **(a)** correspond to those obtained using a K content in organic matter ($[K]_{bio}$) taken from the compilation of Charbonnier *et al*. (2020) and those in **(b)** rely on the use of the chemical composition of leaf reference materials.

Supplementary Information References

Abbe, T.B., Montgomery, D.R. (2003) Patterns and processes of wood debris accumulation in the Queets river basin, Washington. *Geomorphology* 51, 81–107. https://doi.org/10.1016/S0169-555X(02)00326-4

Bouchez, J., Gaillardet, J., France-Lanord, C., Maurice, L., Dutra-Maia, P. (2011) Grain size control of river suspended sediment geochemistry: Clues from Amazon River depth profiles. *Geochemistry, Geophysics, Geosystems* 12, Q03008. https://doi.org/10.1029/2010GC003380

Bouchez, J., von Blanckenburg, F., Schuessler, J.A. (2013) Modeling novel stable isotope ratios in the weathering zone. *American Journal of Science* 313, 267–308. https://doi.org/10.2475/04.2013.01

Bridgestock, L., Hsieh, Y.-T., Porcelli, D., Homoky, W.B., Bryan, A., Henderson, G.M. (2018) Controls on the barium isotope compositions of marine sediments. *Earth and Planetary Science Letters* 481, 101–110. https://doi.org/10.1016/j.epsl.2017.10.019

Bridgestock, L., Hsieh, Y.-T., Porcelli, D., Henderson, G.M. (2019) Increased export production during recovery from the Paleocene–Eocene thermal maximum constrained by sedimentary Ba isotopes. *Earth and Planetary Science Letters* 510, 53–63. https://doi.org/10.1016/j.epsl.2018.12.036

Bridgestock, L., Nathan, J., Paver, R., Hsieh, Y.-T., Porcelli, D., Tanzil, J., Holdship, P., Carrasco, G., Annammala, K.V., Swarzenski, P.W., Henderson, G.M. (2021) Estuarine processes modify the isotope composition of dissolved riverine barium fluxes to the ocean. *Chemical Geology* 579, 120340. https://doi.org/10.1016/j.chemgeo.2021.120340

Brimhall, G.H., Lewis, C.J., Ford, C., Bratt, J., Taylor, G., Warin, O. (1991) Quantitative geochemical approach to pedogenesis: importance of parent material reduction, volumetric expansion, and eolian influx in lateritization. *Geoderma* 51, 51–91. https://doi.org/10.1016/0016-7061(91)90066-3

Bullen, T., Chadwick, O. (2016) Ca, Sr and Ba stable isotopes reveal the fate of soil nutrients along a tropical climosequence in Hawaii. *Chemical Geology* 422, 25–45. https://doi.org/10.1016/j.chemgeo.2015.12.008

Cao, Z., Siebert, C., Hathorne, E.C., Dai, M., Frank, M. (2020) Corrigendum to "Constraining the oceanic barium cycle with stable barium isotopes" [Earth Planet. Sci. Lett. 434 (2016) 1–9]. *Earth and Planetary Science Letters* 530, 116003. https://doi.org/10.1016/j.epsl.2019.116003

Charbonnier, Q., Moynier, F., Bouchez, J. (2018) Barium isotope cosmochemistry and geochemistry. *Science Bulletin* 63, 385–394. https://doi.org/10.1016/j.scib.2018.01.018

Charbonnier, Q., Bouchez, J., Gaillardet, J., Gayer, É. (2020) Barium stable isotopes as a fingerprint of biological cycling in the Amazon River basin. *Biogeosciences* 17, 5989–6015. https://doi.org/10.5194/bg-17-5989-2020

Charbonnier, Q., Bouchez, J., Gaillardet, J., Calmels, D., Dellinger, M. (2022) The influence of black shale weathering on riverine barium isotopes. *Chemical Geology* 594, 120741. https://doi.org/10.1016/j.chemgeo.2022.120741

Chaudhuri, S., Clauer, N., Semhi, K. (2007) Plant decay as a major control of river dissolved potassium: A first estimate. *Chemical Geology* 243, 178–190. https://doi.org/10.1016/j.chemgeo.2007.05.023

Chetelat, B., Liu, C.Q., Zhao, Z.Q., Wang, Q.L., Li, S.L., Li, J., Wang, B.L. (2008) Geochemistry of the dissolved load of the Changjiang Basin rivers: Anthropogenic impacts and chemical weathering. *Geochimica et Cosmochimica Acta* 72, 4254–4277. https://doi.org/10.1016/j.gca.2008.06.013

Curtis, P.G., Slay, C.M., Harris, N.L., Tyukavina, A., Hansen, M.C. (2018) Classifying drivers of global forest loss. *Science* 361, 1108–1111. https://doi.org/10.1126/science.aau3445

Dellinger, M., Gaillardet, J., Bouchez, J., Calmels, D., Galy, V., Hilton, R.G., Louvat, P., France-Lanord, C. (2014) Lithium isotopes in large rivers reveal the cannibalistic nature of modern continental weathering and erosion. *Earth and Planetary Science Letters* 401, 359–372. https://doi.org/10.1016/j.epsl.2014.05.061

Dellinger, M., Bouchez, J., Gaillardet, J., Faure, L. (2015a) Testing the Steady State Assumption for the Earth's Surface Denudation Using Li Isotopes in the Amazon Basin. *Procedia Earth and Planetary Science* 13, 162–168. https://doi.org/10.1016/j.proeps.2015.07.038

Dellinger, M., Gaillardet, J., Bouchez, J., Calmels, D., Louvat, P., Dosseto, A., Gorge, C., Alanoca, L., Maurice, L. (2015b) Riverine Li isotope fractionation in the Amazon River basin controlled by the weathering regimes. *Geochimica et Cosmochimica Acta* 164, 71–93. https://doi.org/10.1016/j.gca.2015.04.042

Dellinger, M., Bouchez, J., Gaillardet, J., Faure, L., Moureau, J. (2017) Tracing weathering regimes using the lithium isotope composition of detrital sediments. *Geology* 45, 411–414. https://doi.org/10.1130/G38671.1

Friedlingstein, P., O'Sullivan, M., Jones, M.W., Andrew, R.M., Hauck, J., *et al.* (2020) Global Carbon Budget 2020. *Earth System Science Data* 12, 3269–3340. https://doi.org/10.5194/essd-12-3269-2020

Gaillardet, J., Dupré, B., Allègre, C.J. (1995) A global geochemical mass budget applied to the Congo Basin rivers: erosion rates and continental crust composition. *Geochimica et Cosmochimica Acta* 59, 3469–3485. https://doi.org/10.1016/0016-7037(95)00230-W

Gaillardet, J., Dupre, B., Allegre, C.J., Négrel, P. (1997) Chemical and physical denudation in the Amazon River Basin. *Chemical Geology* 142, 141–173. https://doi.org/10.1016/S0009-2541(97)00074-0

Gaillardet, J., Dupré, B., Allègre, C.J. (1999a) Geochemistry of large river suspended sediments: silicate weathering or recycling tracer? *Geochimica et Cosmochimica Acta* 63, 4037–4051. https://doi.org/10.1016/S0016-7037(99)00307-5

Gaillardet, J., Dupré, B., Louvat, P., Allègre, C.J. (1999b) Global silicate weathering and CO_2 consumption rates deduced from the chemistry of large rivers. *Chemical Geology* 159, 3–30. https://doi.org/10.1016/S0009-2541(99)00031-5

Gaillardet, J., Viers, J., Dupré, B. (2014) 7.7 - Trace Elements in River Waters. In: Holland, H.D., Turekian, K.K. (Eds.) *Treatise on Geochemistry*. Second Edition, Elsevier, Amsterdam, 195–235. https://doi.org/10.1016/B978-0-08-095975-7.00507-6

Galy, V., France-Lanord, C., Lartiges, B. (2008) Loading and fate of particulate organic carbon from the Himalaya to the Ganga-Brahmaputra delta. *Geochimica et Cosmochimica Acta* 72, 1767–1787. https://doi.org/10.1016/j.gca.2008.01.027

Galy, V., Peucker-Ehrenbrink, B., Eglinton, T. (2015) Global carbon export from the terrestrial biosphere controlled by erosion. *Nature* 521, 204–207. https://doi.org/10.1038/nature14400

Garçon, M., Chauvel, C., France-Lanord, C., Limonta, M., Garzanti, E. (2014) Which minerals control the Nd–Hf–Sr–Pb isotopic compositions of river sediments? *Chemical Geology* 364, 42–55. https://doi.org/10.1016/j.chemgeo.2013.11.018

Gou, L.F. *et al.* (2020) Seasonal riverine barium isotopic variation in the middle Yellow River: Sources and fractionation. *Earth and Planetary Science Letters* 531, 115990. https://doi.org/10.1016/j.epsl.2019.115990

Guay, C.K., Falkner, K.K. (1998) A survey of dissolved barium in the estuaries of major Arctic rivers and adjacent seas. *Continental Shelf Research* 18, 859–882. https://doi.org/10.1016/S0278-4343(98)00023-5

Hansen, M.C. *et al.* (2013) High-Resolution Global Maps of 21st-Century Forest Cover Change. *Science* 342, 850–853. https://doi.org/10.1126/science.1244693. Data available on-line from: http://earthenginepartners.appspot.com/science-2013-global-forest.

Heartsill Scalley, T., Scatena, F.N., Moya, S., Lugo, A.E. (2012) Long-term dynamics of organic matter and elements exported as coarse particulates from two Caribbean montane watersheds. *Journal of Tropical Ecology* 28, 127–139. https://doi.org/10.1017/S0266467411000733

Henchiri, S., Gaillardet, J., Dellinger, M., Bouchez, J., Spencer, R.G.M. (2016) Riverine dissolved lithium isotopic signatures in low-relief central Africa and their link to weathering regimes. *Geophysical Research Letters* 43, 4391–4399. https://doi.org/10.1002/2016GL067711

Holmes, R.M. *et al.* (2012) Seasonal and Annual Fluxes of Nutrients and Organic Matter from Large Rivers to the Arctic Ocean and Surrounding Seas. *Estuaries and Coasts* 35, 369–382. https://doi.org/10.1007/s12237-011-9386-6

Horner, T.J., Kinsley, C.W., Nielsen, S.G. (2015) Barium-isotopic fractionation in seawater mediated by barite cycling and oceanic circulation. *Earth and Planetary Science Letters* 430, 511–522. https://doi.org/10.1016/j.epsl.2015.07.027

Lemarchand, D., Gaillardet, J., Lewin, E., Allegre, C.J. (2000) The influence of rivers on marine boron isotopes and implications for reconstructing past ocean pH. *Nature* 408, 951–954. https://doi.org/10.1038/35050058

Li, X., Han, G., Liu, M., Liu, J., Zhang, Q., Qu, R. (2022) Potassium and its isotope behaviour during chemical weathering in a tropical catchment affected by evaporite dissolution. *Geochimica et Cosmochimica Acta* 316, 105–121. https://doi.org/10.1016/j.gca.2021.10.009

Mikkelsen, R.L. (2007) Managing potassium for organic crop production. *HortTechnology* 17, 455–460. https://doi.org/10.21273/HORTTECH.17.4.455

Milliman, J.D., Farnsworth, K.L. (2011) *River Discharge to the Coastal Ocean: A Global Synthesis*. First Edition, Cambridge University Press, Cambridge. https://doi.org/10.1017/CBO9780511781247

Miyazaki, T., Kimura, J.-I., Chang, Q. (2014) Analysis of stable isotope ratios of Ba by double-spike standard-sample bracketing using multiple-collector inductively coupled plasma mass spectrometry. *Journal of Analytical Atomic Spectrometry* 29, 483–490. https://doi.org/10.1039/c3ja50311a

Nan, X.-Y., Yu, H.-M., Rudnick, R.L., Gaschnig, R.M., Xu, J., Li, W.-Y., Zhang, Q., Jin, Z.-D., Li, X.-H., Huang, F. (2018) Barium isotopic composition of the upper continental crust. *Geochimica et Cosmochimica Acta* 233, 33–49. https://doi.org/10.1016/j.gca.2018.05.004

Pan, Y. *et al.* (2011) A Large and Persistent Carbon Sink in the World's Forests. *Science* 333, 988–993. https://doi.org/10.1126/science.1201609

Potter, P.E. (1978) Petrology and Chemistry of Modern Big River Sands. *The Journal of Geology* 86, 423–449. https://doi.org/10.1086/649711

Rudnick, R.L., Gao, S. (2014) 4.1 - Composition of the Continental Crust. In: Holland, H.D., Turekian, K.K. (Eds.) *Treatise on Geochemistry*. Second Edition, Elsevier, Amsterdam, 1–51. https://doi.org/10.1016/B978-0-08-095975-7.00301-6

Spencer, R.G.M. *et al*. (2012) An initial investigation into the organic matter biogeochemistry of the Congo River. *Geochimica et Cosmochimica Acta* 84, 614–627. https://doi.org/10.1016/j.gca.2012.01.013

Stallard, R.F. (1995) Tectonic, Environmental, and Human Aspects of Weathering and Erosion: A Global Review using a Steady-State Perspective. *Annual Review of Earth and Planetary Sciences* 23, 11–39. https://doi.org/10.1146/annurev.ea.23.050195.000303

Taylor, S.R., McLennan, S.M. (1995) The geochemical evolution of the continental crust. *Reviews of Geophysics* 33, 241–265. https://doi.org/10.1029/95RG00262

Tipper, E.T., Galy, A., Gaillardet, J., Bickle, M.J., Elderfield, H., Carder, E.A. (2006) The magnesium isotope budget of the modern ocean: Constraints from riverine magnesium isotope ratios. *Earth and Planetary Science Letters* 250, 241–253. https://doi.org/10.1016/j.epsl.2006.07.037

Tipper, E.T., Gaillardet, J., Galy, A., Louvat, P., Bickle, M.J., Capmas, F. (2010) Calcium isotope ratios in the world's largest rivers: A constraint on the maximum imbalance of oceanic calcium fluxes. *Global Biogeochemical Cycles* 24, GB3019. https://doi.org/10.1029/2009GB003574

Uhlig, D., Schuessler, J.A., Bouchez, J., Dixon, J.L., von Blanckenburg, F. (2017) Quantifying nutrient uptake as driver of rock weathering in forest ecosystems by magnesium stable isotopes. *Biogeosciences* 14, 3111–3128. https://doi.org/10.5194/bg-14-3111-2017

van Zuilen, K., Nägler, T.F., Bullen, T.D. (2016) Barium Isotopic Compositions of Geological Reference Materials. *Geostandards and Geoanalytical Research* 40, 543–558. https://doi.org/10.1111/ggr.12122

Viers, J., Dupré, B., Gaillardet, J. (2009) Chemical composition of suspended sediments in World Rivers: New insights from a new database. *Science of The Total Environment* 407, 853–868. https://doi.org/10.1016/j.scitotenv.2008.09.053

Wang, Q.L., Chetelat, B., Zhao, Z.Q., Ding, H., Li, S.L., Wang, B.L., Li, J., Liu, X.L. (2015) Behavior of lithium isotopes in the Changjiang River system: Sources effects and response to weathering and erosion. *Geochimica et Cosmochimica Acta* 151, 117–132. https://doi.org/10.1016/j.gca.2014.12.015

Wittmann, H., Oelze, M., Gaillardet, J., Garzanti, E., von Blanckenburg, F. (2020) A global rate of denudation from cosmogenic nuclides in the Earth's largest rivers. *Earth-Science Reviews* 204, 103147. https://doi.org/10.1016/j.earscirev.2020.103147

Wohl, E., Dwire, K., Sutfin, N., Polvi, L., Bazan, R. (2012) Mechanisms of carbon storage in mountainous headwater rivers. *Nature Communications* 3, 1263. https://doi.org/10.1038/ncomms2274